Nanoparticles

Atomic-Scale Characterization of Aluminum-Based Multishell Nanoparticles Created by Solid-State Synthesis**

*Christian Monachon, David C. Dunand, and David N. Seidman**

Many metallic alloys contain nanoparticles created by solid-state precipitation and, to date, these nanoparticles show simple chemical structures (either homogenous or core–shell). Creating more-complex nanoparticles in metallic alloys (e.g., particles with a core surrounded by multiple concentric shells) would be interesting for two reasons. First, this would represent a proof of concept of a generic, solid-state approach based on a simple heat treatment, applicable to a large variety of metallic and nonmetallic systems with particular characteristics (i.e., a matrix with solubility for solute elements varying with temperature whose diffusion kinetics are mismatched).[1,2] Second, in the field of structural metallic alloys, such complex, tailored nanoparticles can better fulfill the often contradictory requirements for particle stiffness, lattice-parameter mismatch, and shearability, which control the elastic interactions of nanoparticles with dislocations (and hence the alloy's strength) and their coarsening resistance via intrinsic diffusivities and interfacial free energies (and hence the alloy's aging resistance).[3–6] While core/multishell nanoparticles have been synthesized in liquid suspensions,[7–11] they have never been created within a solid matrix to the best of our knowledge. Core/single-shell particles form in aluminum alloys upon heat treatment; for example, Al_3(Sc, rare earth (RE)) nanoparticles with RE-rich cores and Sc-rich shells[2,12] and Al_3(Li, Sc) particles with Al_3(Sc, Li) cores and Al_3Li shells.[3,13] In this Communication, we present a general methodology for synthesizing nanoparticles with a core and two concentric shells, which we demonstrate for a quaternary Al–Li–Sc–RE alloy by combining the methods used to create single-shell nanoparticles in ternary Al–Sc–RE,[2,12] and Al–Li–Sc alloys.[3,13] Here, core/double-shell nanoparticles were obtained by applying the following heat treatment to an Al–6.3Li–0.069Sc–0.018Yb alloy: a) homogenization at 640°C followed by quenching in an iced brine, b) aging at 325°C for 8 h, followed by quenching down to 170°C, and c) aging for one week at this temperature and quenching in ice brine.

Scanning electron microscopy (SEM) observations after the 640°C homogenization step detected primary particles (≈1–5 μm in size) at grain boundaries containing Sc, Yb, and Li. As a result, the α-Al matrix had a somewhat depleted composition of Al–5.5Li–0.055Sc–0.008Yb as measured by atom-probe tomography (APT) performed immediately after homogenization. The first 325°C aging step avoids the formation of the stable AlLi δ-phase (with the B_{32} structure[14]), while providing a large thermodynamic driving force for homogenously distributed precipitates of core/shell Al_3X (L_{12}) nanoparticles, where X can be Li, Sc, and/or Yb, as all three binary L_{12} trialuminides exist.[4,15,16] The second 170°C aging step was performed close to the metastable δ'-Al_3Li solvus curve[17] to minimize the thermodynamic driving force for homogeneous nucleation and thereby enhance heterogeneous nucleation of δ'-Al_3Li as a second shell on the pre-existing core/shell Al_3X particles.

The alloy's microhardness was 725 ± 10 MPa after the first 325°C aging step and 960 ± 20 MPa after the second 170°C step, confirming that the nanoparticles precipitated after each treatment are effective strengtheners of pure aluminum with a microhardness of ≈200 MPa. The nanoparticles obtained at 325°C cannot be observed by dark-field transmission electron microscopy (DF-TEM) as their structure factor is zero due to their particular composition.[15,18,19] The nanoparticles obtained subsequently at 170°C had a spheroidal morphology (Figure 1) and a mean diameter of 12.2 ± 0.3 nm.

The two-step aging procedure resulted in two distinct populations of nanoparticles, as detected by APT for the >130 million atoms collected. A total of 208 nanoparticles with

[*] Prof. D. N. Seidman
Department of Materials Science and Engineering
Northwestern University
Northwestern University Center for Atom-Probe Tomography (NUCAPT)
2220 Campus Drive, Evanston, IL 60208 (USA)
E-mail: d-seidman@northwestern.edu
C. Monachon,[+] Prof. D. C. Dunand
Department of Materials Science and Engineering
Northwestern University
2220 Campus Drive, Evanston, IL 60208 (USA)
[+] Current address: Swiss Federal Institute of Technology, Lausanne (EPFL), CH-1015 Lausanne, Switzerland

[**] C.M. is grateful to Prof. A. Mortensen (EPFL) for his support for performing M.S. thesis research at Northwestern and Mr. M. E. Krug (Northwestern University) for experimental assistance. This research is supported by the U.S. Department of Energy through grant DE–FG02–98ER45721. Atom-probe tomography measurements were performed in the Northwestern University Center for Atom-Probe Tomography (NUCAPT). The LEAP tomography system was purchased and upgraded with funding from NSF-MRI (DMR-0420532) and ONR-DURIP (N00014-0400798, N00014-0610539, and N00014-0910781) grants.

DOI: 10.1002/smll.201000325

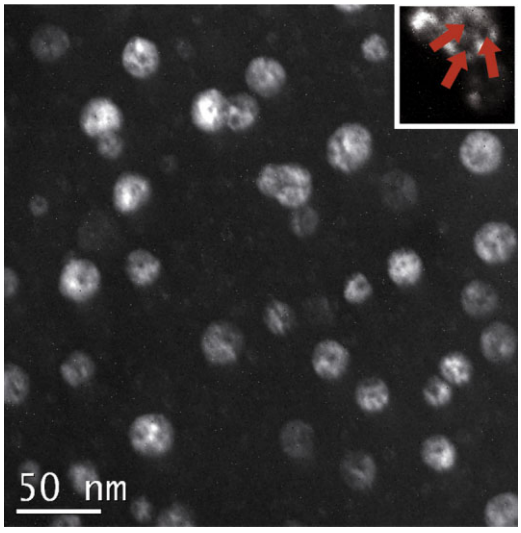

Figure 1. DF-TEM image of δ'-Al_3Li nanoparticles precipitated within the α-Al matrix (using a 100 superlattice reflection on a <110> zone axis) illustrating their spheroidal morphology and their average diameter of 12.2 nm. The inset figure shows smaller, dark Al_3(Li,Sc,Yb) nanoparticles created previously at 325 °C (arrows) that either overlap with or constitute the core of the larger and brighter δ'-Al_3Li nanoparticles. Discrimination between these two scenarios is impossible due to a structure factor that is zero for the Al_3(Li,Sc,Yb) nanoparticles formed at 325 °C, which results from the simultaneous presence of Li, Sc, and Yb on the same L_{12} sublattice site.

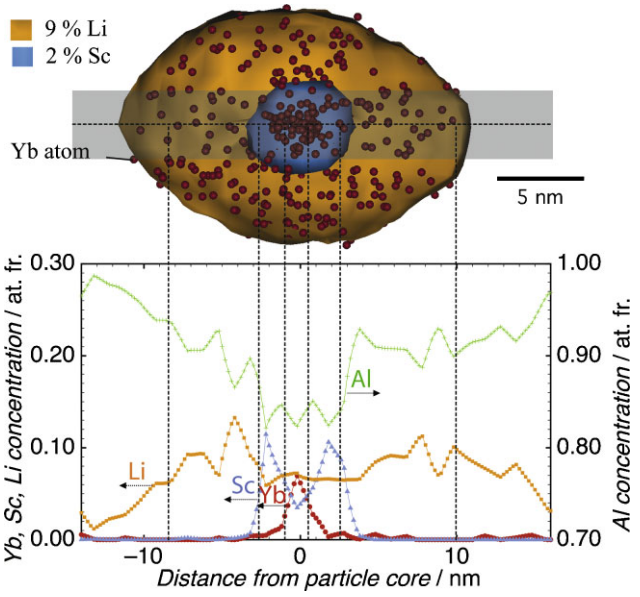

Figure 2. Example of a core/double-shell nanoparticle analyzed by atom-probe tomography and reconstructed using IVAS (Imago Scientific Instruments). The concentration profiles are parallel to the long axis of the tip and exhibit a Yb-rich Al_3(Li,Yb,Sc) core, a Sc-rich Al_3(Li,Sc,Yb) first shell, and a δ'-Al_3Li second shell nearly free of Sc and Yb. A single proximity histogram[29] averaging the 12 nanoparticles cannot be calculated as their cores and shells exhibit nonuniform thicknesses.

Sc-rich shells and Yb-rich cores were detected, with 1:1 Li/Sc and 1:0.29 Sc/Yb ratios (averaged over the whole particle volume) and an average diameter of 2.2 ± 0.8 nm. Additionally, twelve core/double-shell nanoparticles were detected, consisting of core/shell nanoparticles with average 1:0.58 Li/Sc and 1:0.30 Sc/Yb ratios embedded within a second outer shell with an average 1:0.25 Al/Li ratio (but probably with the δ'-Al_3Li composition, as inferred from the strong contrast in the DF-TEM micrographs).

Figure 2 shows an example of such a core/double-shell nanoparticle as determined by APT. The spindle-shaped morphology of the outer shell is an "inverse magnification" artifact, which is sometimes observed in APT studies of two-phase alloys:[20,21] the evaporation field of the δ'-Al_3Li phase is smaller than that of the α-Al matrix resulting in an artificial reduction of the diameter of the δ'-Al_3Li nanoparticles in the directions perpendicular to the long axis of the microtip. The true spheroidal shape of the nanoparticles is, however, visible in the DF-TEM images (Figure 1). Furthermore, this effect underestimates the Li concentration in the core and the shells, preventing precise quantification of the Li concentration.

The concentration profiles obtained from a 2-nm-radius analysis cylinder parallel to the tip axis placed through each nanoparticle in the dataset recorded by APT (as illustrated in the top of Figure 2) are reproducible to within ±20% among the twelve core/double-shell nanoparticles detected. A representative example is given in Figure 2, where the central core region has a diameter of ≈3.3 nm and an average composition of $Al_{0.833}(Li_{0.070}Yb_{0.052}Sc_{0.045})$. In this core, the Li concentration (yellow in Figure 2, and probably underestimated, as discussed above) is nearly constant at 6.4 at% and the Yb concentration (red) exhibits an approximately Gaussian-shaped symmetrical profile with a maximum value of 6.8 at%. The Sc concentration profile is symmetrical with respect to a local minimum value of 3.6 at% at the core's center, where the Yb concentration is highest, suggesting that both Yb and Sc are located on the same Li sublattice of the L_{12} structure. Surrounding the core of this nanoparticle, the first shell has an average thickness of 1.8 nm and a mean composition of $Al_{0.832}(Li_{0.090}Sc_{0.063}Yb_{0.015})$ and thus contains more Sc and less Yb than the core. The Sc concentration profiles have maxima immediately adjacent to the interface between the first and second shells. Finally, the second shell, engulfing both the core and the first shell, has an average thickness of 10 nm and consists almost exclusively of Al and Li atoms, which both have nonuniform concentration profiles. The mean composition of the second shell is $Al_{0.88}(Li_{0.119}\ Sc_{0.001}Yb_{0.001})$ but is probably close to the Al_3Li composition, as discussed previously. Surrounding this complex nanoparticle is the α-Al matrix with a mean composition of Al–3.5Li–0.002Sc–0.004Yb. Thus, the analysis of the concentration profiles (Figure 2) yields a clear and detailed chemical picture of a core/double-shell nanoparticle, which was produced by a scientifically-designed two-step aging protocol.

Figure 3 shows an unusual nanoparticle displaying two cores with concentration profiles similar to the single-core particles (Figure 2). This double-core nanoparticle, which resembles a "double-yolk egg," is the only one within the twelve core/double-shell particles[21] observed and thus probably represents a minor, though measurable, subpopulation. It was most likely formed when the outer δ' shells on two closely adjacent nanoparticles coalesced. The center-to-center distance between the two cores is 7.2 nm and the diameters of the

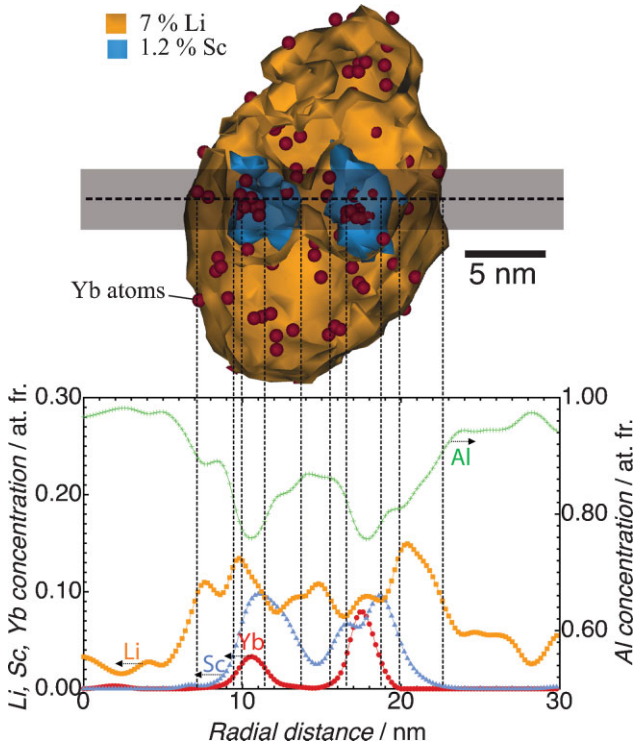

Figure 3. APT reconstruction of a "double-yolk egg" nanoparticle containing two Yb-rich Al_3(Li,Yb,Sc) cores, which are surrounded by their respective Sc-rich Al_3(Li,Sc,Yb) first shells and a common δ'-Al_3Li second outer shell. The concentration profiles have the same colors as in Figure 2 and are perpendicular to the long axis of the tip.

left-hand (LH) and right-hand (RH) cores are 2.1 and 2.3 nm, respectively. The Yb concentration profile displays maxima in each of the cores and the Li and Sc concentration profiles are complex. The average compositions, based on the concentration profiles, of the LH core [$Al_{0.77}(Li_{0.11}Sc_{0.09}Yb_{0.03})$] and RH core [$Al_{0.77}(Li_{0.09}$ $Sc_{0.07}Yb_{0.07})$] are approximately the same within the expected experimental error given the small numbers of Sc and Yb atoms in the cores (typically 10–20 each). The first shells surrounding the two cores in Figure 3 have average thicknesses of 1.4 nm (LH) and 1.7 nm (RH), respectively, and mean compositions of $Al_{0.86}(Li_{0.07}$ $Sc_{0.05}Yb_{0.02})$ and $Al_{0.86}(Li_{0.06}Sc_{0.05}Yb_{0.03})$, respectively. The single second shell consists mainly of Al and Li atoms with nonuniform concentration profiles.

We believe this to be the first report of core/double-shell nanoparticles in an Al-based alloy or, indeed, in any metallic matrix. This complex nanostructure is made possible by the choice of alloying elements with disparate solubilities and concentration-dependent intrinsic diffusivities, D_i, in Al. The first heat treatment at 325°C produces nanoparticles with a core richer in the faster-diffusing Yb and a shell richer in the slower-diffusing Sc, while the highly soluble Li remains mostly in solution but is coprecipitated in small amounts in the core and first shell. The second heat treatment at 170°C, where the Li solubility is exceeded, results in heterogeneous nucleation and precipitation of Al_3Li as a second shell on the initial core/shell nanoparticles at rates that are experimentally attainable despite the much lower temperature given the high concentration-dependent intrinsic diffusivity of Li in aluminum. This strategy is general and, in principle, could be used on other Al-based alloys (e.g., Al–Li–Sc–Ti, where $D_{Li} > D_{Sc} > D_{Ti}$ or Al–Er–Sc–Zr, where $D_{Er} > D_{Sc} > D_{Zr}$), or other alloys (e.g., Ni–Al–Cr–W, where $D_{Al} > D_{Cr} > D_{W}$), with temperatures selected to create the necessary sequential core and shells in the nanoparticles: the required condition on the D_i values is necessary but not sufficient. Here, Li, Sc, and Yb are chosen also because they create trialuminide phases with the same $L1_2$ crystal structure with partial or complete mutual solubilities.[2,22,23] However, even when this condition is fulfilled, the aging temperatures must be carefully chosen to create multiple shells: for instance, in Al–0.13Sc–0.13Hf–0.02Zr, where the condition $D_{Sc} > D_{Zr} > D_{Hf}$ is fulfilled and where all three trialuminides exist, nanoparticles with Al_3Sc cores surrounded by a single Al_3(Sc, Zr, Hf) shell were observed.[24] Similarly, in an Al–6.3Li–0.36Sc–0.13Zr alloy (where $D_{Li} > D_{Sc} > D_{Zr}$ and the three trialuminides exist), a two-step aging treatment nucleated δ'-Al_3Li shells at 190°C on Al_3(Sc, Zr) cores initially created at 450°C,[15] whose Zr segregation at the outside of the core is, however, too weak to qualify as an independent shell.

To conclude, an Al–Li-solid solution containing small additions of Sc and Yb was subjected to a two-step heat-treatment protocol resulting in nucleation and growth of spheroidal Al_3(Li, Sc, Yb) nanoparticles with complex radial concentration profiles corresponding to a core surrounded by two concentric shells. APT revealed that the nanoparticles consist of a central Yb-rich core, a first Sc–rich inner shell (created simultaneously at 325°C), and a second Li-rich outer shell (produced subsequently at 170°C). Also, a double-yolk-egg nanoparticle was detected, consisting of a single outer shell containing two cores with their respective inner shells and is relevant both as an example of the limitation of the control of nanoscopic features that the present technique provides (if uniform particles are desired) and as a new type of multicore/multishell nanoparticle. The obtained nanoparticles strengthen the Al–Li matrix and their radially layered core/double-shell structure (with single or double cores) permits considerable freedom for: i) tailoring their interactions with matrix dislocations, which determines an alloy's strength, and ii) decreasing their coarsening kinetics, which improves an alloy's resistance to overaging at elevated temperatures. Finally, still in the field of physical metallurgy, other systems have been presented that have the potential to yield particles with even increased complexity that are still based on the approach and synthesis route devised in this paper.

Experimental Section

Aging: The Al–6.3Li–0.069Sc–0.018Yb alloy (hereafter all concentrations are given in at%), whose composition was measured by direct-coupled plasma mass spectroscopy (Wah-Chang ATI), was cast from pure elements. The following aging protocol was utilized: a) homogenization at 640°C for 72 h in molten LiCl terminated by quenching into iced brine, b) aging at 325°C for 8 h in a molten-salt bath ($NaNO_2$:$NaNO_3$:KNO_3), followed by quenching in a 170°C oil bath, and c) aging at this temperature for one week and then water quenching.

Microhardness: Vickers microhardness tests were made using a Struers Duramin-1 using 20 gf load for 10 s.

DF-TEM: DF-TEM observations were performed using a Hitachi H8100 TEM utilizing superlattice reflections. First, 3-mm-diameter specimens were punched from a 250-μm-thick foil and were then mechanically polished to a thickness of 80–100 μm. The specimens were made electron transparent using a Struers Tenupol 5 electropolisher with an electrolyte consisting of 33% nitric acid and 66% methanol maintained at –30°C and 12–14 V with direct current (DC).

APT observations: Needle-shaped specimens[25–27] were created by a two-step electropolishing procedure utilizing a solution of 10% perchloric acid in acetic acid, followed by a 2% perchloric acid in butoxyethanol solution at voltages between 7 and 14 V_{DC}.[28] The resulting microtips were analyzed utilizing a three-dimensional (3D) local-electrode atom probe (LEAP) 3000X Si tomography system (Imago Scientific Instruments) at a tip temperature of 25 ± 0.5 K, a voltage pulse repetition rate of 250 kHz, and a 16% pulse fraction (pulse voltage/stationary-state DC voltage). The pressure in the ultrahigh-vacuum 3D LEAP tomography system during analyses was 5×10^{-11} Torr. Data analyses were performed using IVAS (versions 3.05 and 3.06, Imago Scientific Instruments).

Keywords:
atom-probe tomography · core–shell precipitates · transmission electron microscopy · trialuminides

[1] K. E. Knipling, D. C. Dunand, D. N. Seidman, *Z. Metallkd.* **2006**, *97*, 246–265.
[2] M. E. van Dalen, R. A. Karnesky, J. R. Cabotaje, D. C. Dunand, D. N. Seidman, *Acta Mater.* **2009**, *57*, 4081–4089.
[3] M. E. Krug, D. C. Dunand, D. N. Seidman, *Appl. Phys. Lett.* **2008**, *92*, 124107.
[4] E. A. Marquis, D. N. Seidman, *Acta Mater.* **2001**, *49*, 1909–1919 .
[5] J. D. Robson, *Acta Mater.* **2004**, *52*, 1409–1412.
[6] J. Røyset, N. Ryum, *Int. Mater. Rev.* **2005**, *50*, 19–44.
[7] G. Zhang, C. Wu, *Adv. Polym. Sci.* **2006**, *195*, 101–176.
[8] K. Nakashima, P. Bahadur, *Adv. Colloid Interface Sci.* **2006**, *123–126*, 75–96.
[9] J. Keilitz, M. R. Radowski, J.-D. Marty, R. Haag, F. Gauffre, C. Mingotaud, *Chem. Mater.* **2008**, *20*, 2423–2425.
[10] Y. Liu, Z. Su, *J. Appl. Polym. Sci.* **2008**, *107*, 2082–2088.
[11] L. Li, E. S. G. Choo, Z. Liu, J. Ding, J. Xue, *Chem. Phys. Lett.* **2008**, *461*, 114–117.
[12] R. A. Karnesky, M. E. van Dalen, D. C. Dunand, D. N. Seidman, *Scripta Mat.* **2006**, *55*, 437–440.
[13] Y. Miura, K. Horikawa, K. Yamada, M. Nakayama, in *Proc. 4th Int. Conf. Aluminum Alloys*, Georgia Institute of Technology, Atlanta, GA, 1994, p. 161–168.
[14] B. Hallstedt, O. Kim, *Int. J. Mater. Res.* **2007**, *98*, 961–969.
[15] V. Radmilovic, A. Tolley, E. A. Marquis, M. D. Rossel, Z. Lee, U. Dahmen, *Scripta Mat.* **2008**, *58*, 529–532.
[16] M. E. van Dalen, D. C. Dunand, D. N. Seidman, *J. Mat. Sci.* **2006**, *41*, 7814–7823.
[17] R. Poduri, L.-Q. Chen, *Acta Metall. Mater.* **1996**, *45*, 245–255.
[18] M. K. Aydinol, A. S. Bor, *J. Mater. Sci.* **1995**, *14*, 1147–1149.
[19] F. W. Gayle, J. B. van der Sande, *Acta Metall. Mater.* **1989**, *37*, 1033–1046.
[20] S. R. Goodman, S. S. Brenner, J. R. Low, *Met. Trans.* **1973**, *4*, 2363–2369.
[21] S. R. Goodman, S. S. Brenner, J. R. Low, *Met. Trans.* **1973**, *4*, 2371–2378.
[22] Y. Harada, D. C. Dunand, *Mater. Sci. Forum* **2007**, *539-543*, 1565–1570.
[23] Y. Harada, D. C. Dunand, *Intermetallics* **2009**, *17*, 17–24.
[24] H. Hallem, W. Lefebvre, B. Forbord, F. Danoixb, K. Marthinsen, *Mater. Sci. Eng. A* **2006**, *421*, 154–160.
[25] D. N. Seidman, *Ann. Rev. Mater. Res.* **2007**, *37*, 127–158.
[26] D. N. Seidman, *Rev. Sci. Instrum.* **2007**, *78*, 1–3.
[27] T. F. Kelly, M. K. Miller, *Rev. Sci. Instrum.* **2007**, *78*, 1–20.
[28] B. W. Krakauer, D. N. Seidman, *Rev. Sci. Instrum.* **1992**, *63*, 4071–4079.
[29] O. C. Hellman, J. A. Vandenbroucke, J. Rüsing, D. Isheim, D. N. Seidman, *Microsc. Microanal.* **2000**, *6*, 437–444.

Received: March 1, 2010
Revised: March 30, 2010
Published online: July 21, 2010

